Chapter 3

Other Experimental Techniques: Electron Microscopy and X-ray

Even though this book focuses on optical properties and related optical spectroscopy techniques, it seems necessary to briefly review some of the other relevant experimental techniques used for characterization of nanomaterials. This is partly because it is essential for nanomaterials to be thoroughly characterized as much as possible using a combination of experimental techniques due to the intrinsic complex nature of nanomaterials. For example, two of the most basic characteristics are size and shape of nanostructures. Another important property is the surface of nanomaterials due to their extremely large surface-to-volume ratio. Furthermore, it is often important to know the crystal structures of the nanomaterials. To study these different properties requires many other experimental methods, besides optical spectroscopy. Examples include electron microscopy, electrochemistry, X-ray based methods such as X-ray diffraction (XRD), X-ray photoelectron spectroscopy (XPS), and extended X-ray absorption fine structure (XAFS). Of course, most of these techniques can be used for investigating bulk materials as well and are not exclusive for nanomaterials. Nonetheless, these techniques are necessary and powerful in disseminating information about nanomaterials.

OPTICAL PROPERTIES AND SPECTROSCOPY OF NANOMATERIALS
© World Scientific Publishing Co. Pte. Ltd.
http://www.worldscibooks.com/nanosci/7093.html

3.1. Microscopy: AFM, STM, SEM and TEM

Structural determination is essential for nanomaterials research. Since the nanostructures are usually too small to be visualized with conventional optical microscopes, it is important to use appropriate tools to adequately characterize their structure and surface in detail at the molecular or atomic level. This is important not only for understanding their fundamental properties but also for exploring their functional and technical performance in technological applications. There are several experimental techniques that can be used to characterize structural and surface properties of nanomaterials either directly or indirectly, e.g. XRD, STM (scanning tunneling microscopy), AFM (atomic force microscopy), SEM (scanning electron microscopy), TEM (transmission electron microscopy), XAS (X-ray absorption spectroscopy), EXAFS, XANES (X-ray absorption near edge structure), EDX (energy dispersive X-ray), XPS, IR (infrared), Raman, and DLS (dynamic light scattering) [1–5]. Some of these techniques are more surface sensitive than others. Some techniques are directly element-specific while others are not. The choice of techniques depends strongly on the information being sought about the material.

3.1.1. *Scanning probe microscopy (SPM): AFM and STM*

Scanning probe microscopy (SPM) represents a group of techniques, including scanning tunneling microscopy (STM), atomic force microscopy (AFM), and chemical force microscopy (CFM), that have been extensively applied to characterize nanostructures with atomic or subatomic spatial resolution [1, 4, 6–8]. A common characteristic of these techniques is that an atom sharp tip scans across the specimen surface and images are formed by either measuring the current flowing through the tip or the force acting on the tip. SPM can be operated in a number of environmental conditions, in a variety of different liquids or gases, allowing direct imaging of inorganic surfaces and organic molecules. It allows viewing and manipulation of objects on the nanoscale and its invention is a major milestone in nanotechnology.

OPTICAL PROPERTIES AND SPECTROSCOPY OF NANOMATERIALS
© World Scientific Publishing Co. Pte. Ltd.
http://www.worldscibooks.com/nanosci/7093.html

For nonconductive nanomaterials, atomic force microscopy (AFM) is a better choice [9, 10]. AFM is based on measuring the force between the tip and the solid surface. The interaction between two atoms is repulsive at short-range and attractive at long-range. The force acting on the tip reflects the distance from the tip atom(s) to the surface atom, thus images can be formed by detecting the force while the tip is scanned across the specimen. A more generalized application of AFM is scanning force microscopy, which can measure magnetic, electrostatic, frictional, or molecular interaction forces allowing for nanomechanical measurements.

A typical AFM setup involves a sharp tip mounted on a microscale cantilever, a laser, a position sensitive detector, a piezoelectric tube (PZT) scanner, and control electronics, as shown in Fig. 3.1 [8]. The cantilever is typically silicon or silicon nitride with a tip radius or curvature on the order of nanometers. When the tip is brought near a sample surface, forces between the tip and the sample lead to a deflection of the cantilever according to Hooke's law. Depending on the situation, forces that are

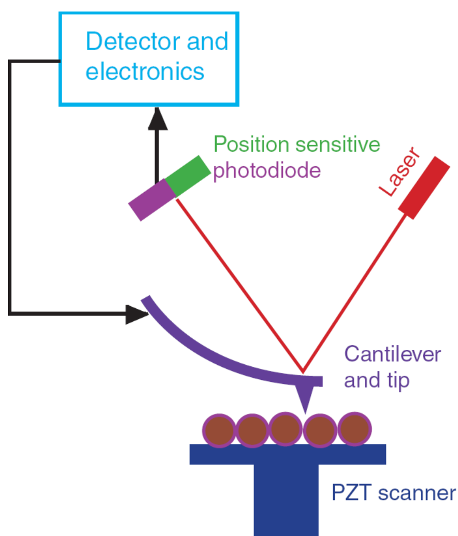

Fig. 3.1. Schematic illustration of the principle of operation underlying atomic force microscopy (AFM).

OPTICAL PROPERTIES AND SPECTROSCOPY OF NANOMATERIALS
© World Scientific Publishing Co. Pte. Ltd.
http://www.worldscibooks.com/nanosci/7093.html

measured in AFM include mechanical contact force, electrostatic forces, chemical bonding, van der Waals forces, capillary forces and magnetic forces. Typically, the deflection is measured using a laser beam reflected from the top of the cantilever into an array of position sensitive photodiodes. To avoid possible collision between the tip and sample surface, a feedback mechanism is often employed to adjust the tip-to-sample distance to maintain a constant force between the tip and the sample. Traditionally, the sample is mounted on a PZT that can move the sample in the z direction for maintaining a constant force and in the x and y directions for scanning the sample. The resulting map of the area $s = f(x,y)$ represents the topography of the sample. The AFM can be operated in a number of modes, depending on the application. In general, possible imaging modes are divided into static (also called contact) modes and a variety of dynamic (or non-contact) modes.

Figure 3.2 shows a frequency modulation (FM)-AFM image obtained with a (111) oriented silicon tip [11]. This image was recorded at positive frequency shift, and thus the forces between the front atom and sample have been repulsive. An advantage of this mode is that the feedback can be set much faster, because the risk of feedback oscillations with a catastrophic tip crash is avoided in this mode. This example clearly shows that AFM is capable of directly providing unprecedentedly detailed information on the atomic scale, which is important for understanding chemical bonding and electronic structure of atoms and molecules.

Another powerful SPM technique is scanning tunneling microscopy (STM), discovered in the 1980s [12]. STM is based on measuring the tunneling current between a sharp metallic tip and specimen. The STM tip does not actually touch the surface of the sample measured. As shown in Fig. 3.3, a voltage is applied between the tip and the specimen, typically between a few mV and a few V. If the tip touches the surface of the specimen, the voltage will result in an electrical current. If the tip is far away from the surface, the current is zero since it is essentially an open circuit. STM operates in the regime of extremely small distances between the tip and the surface of only 0.5 to 1.0 nm, or only a few atomic diameters. At these distances, electrons can tunnel from the probe tip to the surface or vice versa, which is why it is named tunneling microscopy. Since tunneling is a weak process, the tunneling current is thus very low.

OPTICAL PROPERTIES AND SPECTROSCOPY OF NANOMATERIALS
© World Scientific Publishing Co. Pte. Ltd.
http://www.worldscibooks.com/nanosci/7093.html

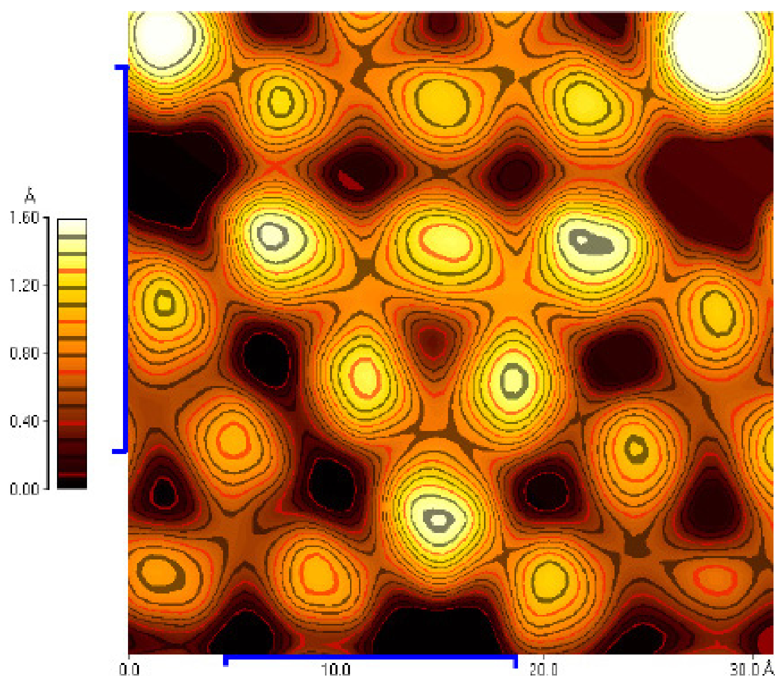

Fig. 3.2. Topographic image of Si(111)–(7 × 7) observed by FM-AFM, imaged with a single crystal silicon tip roughly oriented in a (111) direction. Reproduced with permission from Ref. 11.

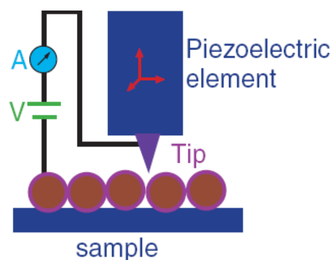

Fig. 3.3. Schematic illustration of the basic operating principle of STM.

STMs typically operate at tunneling currents between a few picoAmperes (pA) and a few nanoAmperes (nA). The tunneling current depends strongly on the distance between the tip and the specimen. Therefore, tunneling current provides a highly sensitive measure of the distance between the tip

OPTICAL PROPERTIES AND SPECTROSCOPY OF NANOMATERIALS
© World Scientific Publishing Co. Pte. Ltd.
http://www.worldscibooks.com/nanosci/7093.html

and the surface. The STM tip is attached to a piezoelectric element used to control the precise distance between the tip and the surface with an electrical voltage. This voltage is adjusted such that the tunneling current is a constant in the z direction, which means that the distance between the tip and the specimen surface is kept at constant. This distance control is achieved using feedback electronics. While distance control is active, the tip can be moved in directions (e.g. x and y) parallel to the sample surface to scan over the surface using two other parts of the piezoelectric element. As the tip scans, the tip needs to be moved in the z direction perpendicular to x and y, through the piezoelectric voltage control, to ensure a constant current. In doing so, the control voltage in the feedback electronics contains information about the surface topology of the specimen. This information is usually transformed into 3D images and plotted on a computer for easy visualization [13]. STM is applicable mainly for conductive samples.

As an example, Fig. 3.4 shows some representative STM topographs of an undecanethiol self-assembled monolayer (SAM) upon UHV annealing at 345 K for 4.5 hours [14]. Figures 3.4 (b)–3.4 (d) are zoom-in images within the area marked in Fig. 3.4(a). The SAM consists of etch-pit free domains up to several hundreds of nanometers in size, with only occasional missing molecules or other point defects. This demonstrates the high spatial resolution capability of STM that is easily on the angstrom scale.

3.1.2. *Electron microscopy: SEM and TEM*

Optical microscopes have limited spatial resolution, usually on the order of a few hundred nm in the best case scenario due to the diffraction limit of light. Higher resolution, a few nm or even sub nm, is needed for many applications, especially in the study of nanomaterials. Scanning electron microscopy (SEM) is a powerful and popular technique for imaging the surfaces of almost any material with a resolution down to about 1 nm [2, 3]. The image resolution offered by SEM depends not only on the property of the electron probe, but also on the interaction of the electron probe with the specimen. The interaction of an incident electron beam with the specimen produces secondary electrons, with energies typically

OPTICAL PROPERTIES AND SPECTROSCOPY OF NANOMATERIALS
© World Scientific Publishing Co. Pte. Ltd.
http://www.worldscibooks.com/nanosci/7093.html

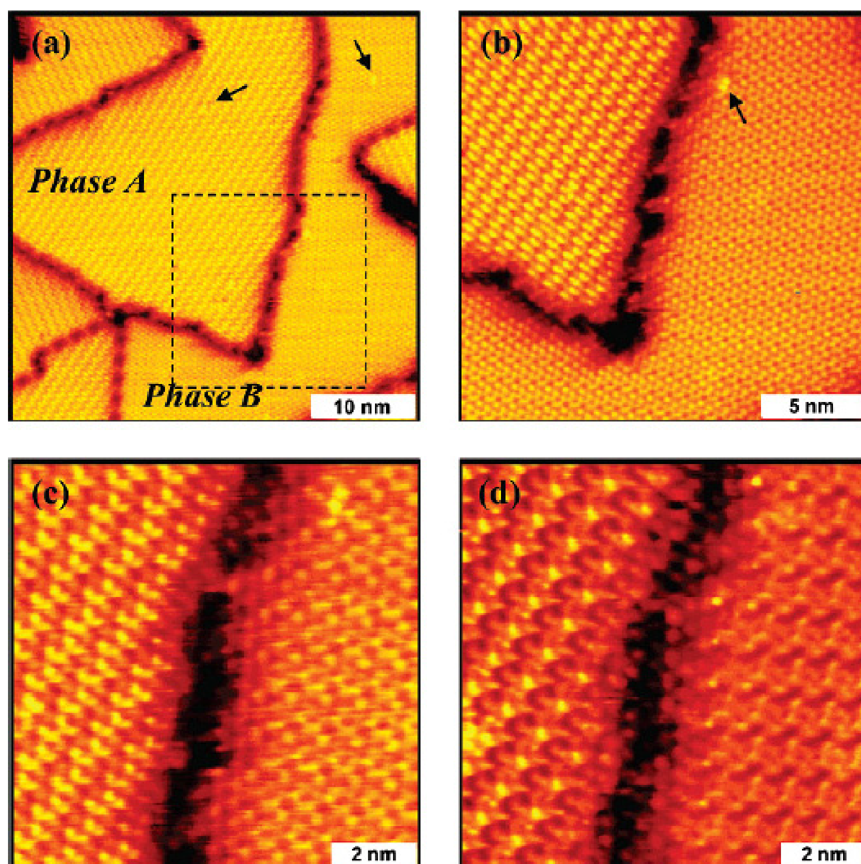

Fig. 3.4. STM topographic images of an undecanethiol self-assembled monolayer (SAM), after annealing at 345 K for 4.5 h under UHV. The images were recorded at (a) 0.8 V, 14 pA; (b) 0.8 V, 14 pA; (c) 0.3 V, 5 pA; (d) 0.3 V, 14 pA. Image (b) was taken inside the square area indicated in panel (a), and panels (c) and (d) are zoomed-in images of panel (b). Point defects in the SAM are indicated by arrows in panels (a) and (b). Two distinct phases, A and B, coexist on the surface, observed simultaneously under the same imaging conditions. Reproduced with permission from Ref. 14.

smaller than 50 eV, the emission efficiency of which sensitively depends on surface geometry, surface chemical characteristics and bulk chemical composition [15]. SEM can thus provide information about the surface topology, morphology and chemical composition. The high resolution

OPTICAL PROPERTIES AND SPECTROSCOPY OF NANOMATERIALS
© World Scientific Publishing Co. Pte. Ltd.
http://www.worldscibooks.com/nanosci/7093.html

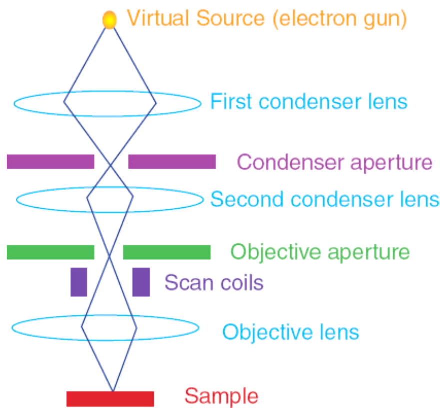

Fig. 3.5. Schematic diagram to illustrate the major components for image formation in a typical scanning electron microscope.

capability afforded by SEM makes it convenient for probing nanomaterials of which the structural features on the nanoscale are critical to their properties and functionalities.

Figure 3.5 shows a schematic of the imaging system in a typical scanning electron microscope starting from the electron source. A stream of monochromatic electrons generated by an electron gun is condensed by the first condenser lens to both form the beam and limit the amount of current, as well as, in conjunction with the condenser aperture, to eliminate the high-angle electrons from the beam. The second condenser lens focuses the electrons into a thin, tight, coherent beam and an objective aperture is used to further eliminate high-angle electrons from the beam. A set of coils is used to scan the beam in a grid fashion. The objective lens focuses the scanning beam onto the specimen desired, one point at a time. Interaction between the electron beam and the sample generates back scattered electrons (BSE), X-ray, secondary electrons (SE), and Auger electrons in a thick or bulk sample. These various electrons are detected and the signal detected contains information about the specimen under investigation. BSE is more sensitive to heavier elements than SE. The X-ray radiation can be detected in a technique called energy dispersive X-ray (EDX) spectroscopy that can be used to identify specific elements [16, 17].

OPTICAL PROPERTIES AND SPECTROSCOPY OF NANOMATERIALS
© World Scientific Publishing Co. Pte. Ltd.
http://www.worldscibooks.com/nanosci/7093.html

As an example, Fig. 3.6 shows SEM images for a MgH_2–Ni nanocomposite material prepared by ball-milling [16]. Such material is of interest for potential hydrogen storage applications. In the secondary electron (SE) micrograph [Fig. 3.6(a)], various sized particles exist in the range of less than 1 μm to more than 5 μm, and the particle size is clearly not very homogeneous. In the back scattering electron (BSE) image [Fig. 3.6(b)], which is the same area as the SE image, small-size particles with <1 μm in diameter are bright and uniformly distributed on the large-size particles. The BSE signals for the heavier element or the composite containing heavier element can be detected as much brighter spots. Therefore, the bright part shows the distribution of Ni particles because Mg has much smaller atomic number. This indicates that the Ni particles homogeneously distribute in such a micrometer scale range on the surface of MgH_2. This example shows that SE and BSE images can differ in the information they can provide.

Transmission electron microscopy (TEM) is a high spatial resolution structural and chemical characterization tool [18]. A modern TEM has the capability to directly image atoms in crystalline specimens at resolutions close to 0.1 nm, smaller than interatomic distance. An electron beam can also be focused to a diameter smaller than ~0.3 nm, allowing quantitative chemical analysis from a single nanocrystal. This type of analysis is extremely important for characterizing materials at a length scale from atoms to hundreds of nanometers. TEM can be used to characterize nanomaterials to gain information about particle size, shape, crystallinity, and interparticle interaction [2, 19].

Figure 3.7 shows a schematic of important components of the image formation system in a typical TEM. Similar to SEM, a stream of monochromatic electrons produced by an electron gun is focused into a small, thin, coherent beam by two condenser lenses. The electron beam is restricted by the condenser aperture to remove high angle electrons before it reaches the specimen. It is important in this case that the specimen is thin enough to allow some electrons to transmit through the sample. Interaction between the electron beam and specimen generates elastically and inelastically scattered electrons, along with some unscattered electrons, in the forward direction after the sample has been detected. The detected signal contains information about the sample. The detection

OPTICAL PROPERTIES AND SPECTROSCOPY OF NANOMATERIALS
© World Scientific Publishing Co. Pte. Ltd.
http://www.worldscibooks.com/nanosci/7093.html

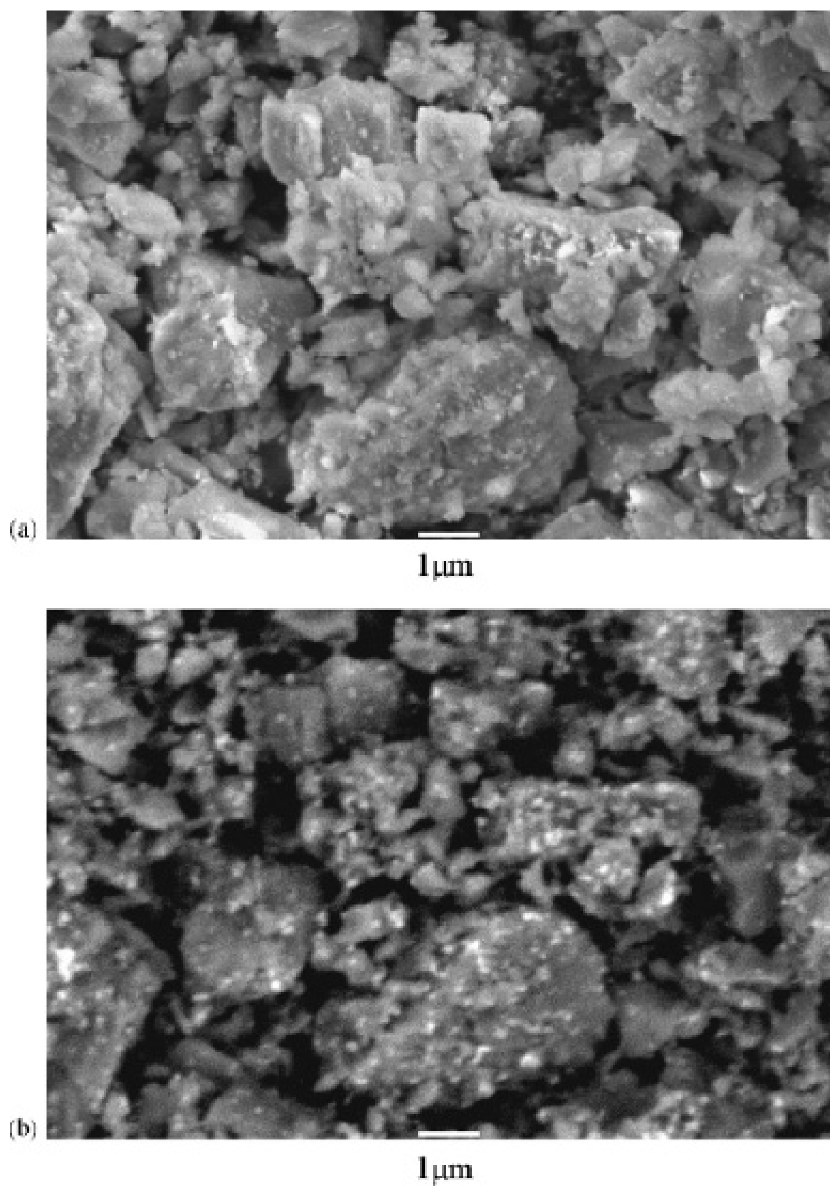

Fig. 3.6. (a) Secondary electron (SE) and (b) back scattering electron (BSE) images of the MgH_2–Ni nanocomposite, in which both (a) and (b) micrographs are taken in the same field. Reproduced with permission from Ref. 16.

OPTICAL PROPERTIES AND SPECTROSCOPY OF NANOMATERIALS
© World Scientific Publishing Co. Pte. Ltd.
http://www.worldscibooks.com/nanosci/7093.html

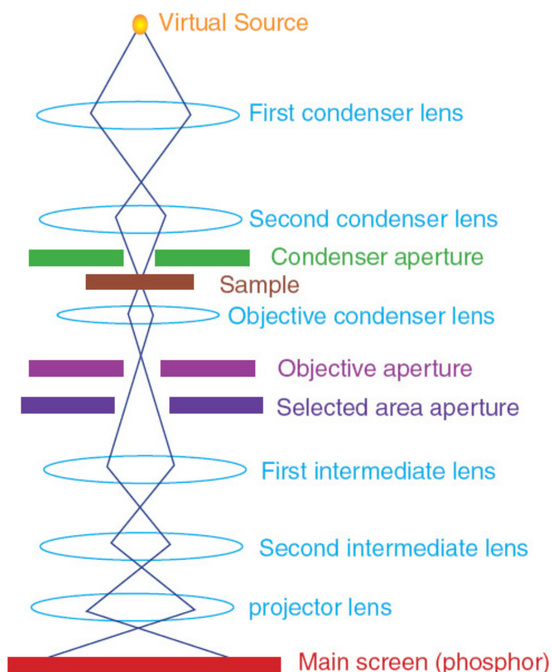

Fig. 3.7. Schematic of major components for image formation of a typical TEM.

involves several lenses to focus the electrons to be detected before they reach the detection phosphor screen. Also shown in the figure are optional objective and selected area metal aperture that can be used to restrict the beam, with the objective aperture enhancing contrast by blocking out high-angle diffracted electrons and the selected area aperture enabling the user to examine the periodic diffraction of electrons by ordered arrangements of atoms in the sample examined. Thus, one major difference between SEM and TEM is that TEM detects "transmitted electrons" and SEM detects "backscattered" and/or secondary electrons. While both techniques can provide topological, morphological and compositional information about the sample, TEM can provide crystallographic information as well. In addition, TEM allows for diffraction patterns to be detected that also contain useful crystallographic information about the sample.

OPTICAL PROPERTIES AND SPECTROSCOPY OF NANOMATERIALS
© World Scientific Publishing Co. Pte. Ltd.
http://www.worldscibooks.com/nanosci/7093.html

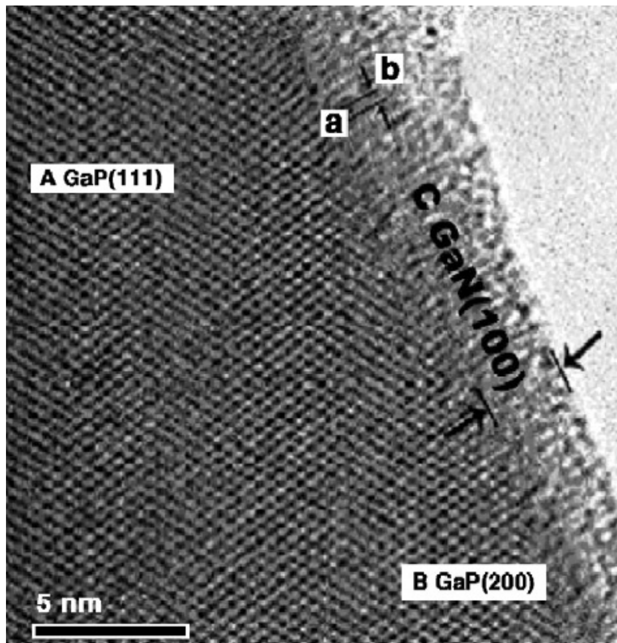

Fig. 3.8. HRTEM image of GaP/GaN core/shell nanocomposite structures clearly showing the boundary between the core and shell. Reproduced with permission from Ref. 20.

Figure 3.8 shows a magnified high resolution TEM (HRTEM) image of GaP/GaN core/shell nanostructures [20]. This image not only clearly shows the crystallographic planes of the core material (GaP) but also the boundary between the core and shell (GaN). Although the shell is mostly amorphous, the lattice planes of some of the areas (e.g. area C) of the shell near the core can also be clearly identified as (100) lattice planes of crystalline GaN. The location "a" measured from the HRTEM image is 0.34 nm, which is larger than that of the GaP(111) and attributed to crystalline grain distortion caused by lattice mismatch between GaP and GaN.

3.2. X-ray: XRD, XPS, and XAFS, SAXS

X-ray diffraction (XRD) is a powerful and routine technique for determining the crystal structure of crystalline materials [21–23]. By examining the diffraction pattern, one can identify the crystalline phase of the material.

OPTICAL PROPERTIES AND SPECTROSCOPY OF NANOMATERIALS
© World Scientific Publishing Co. Pte. Ltd.
http://www.worldscibooks.com/nanosci/7093.html

Small angle scattering is useful for evaluating the average interparticle distance while wide-angle diffraction is useful for refining the atomic structure of nanoclusters [24]. The widths of the diffraction lines are closely related to the size, size distribution, defects and strain in nanocrystals. As the size of the nanocrystals decreases, the line width is broadened due to loss of long range order relative to the bulk. This XRD line width can be used to estimate the size of the particle via the Debye–Scherrer formula.

$$D = \frac{0.9\lambda}{\beta \cos\theta} \tag{3.1}$$

where D is the nanocrystal diameter, λ is the wavelength of light, β is the full width half at maximum (FWHM) of the peak in radians, and θ is the Bragg angle.

Figure 3.9 shows XRD patterns of Fe^{3+} doped TiO_2 (xFe-TiO_2) as well as N and Fe^{3+} doped TiO_2 (N-xFe-TiO_2) with different Fe^{3+} doping concentration [25]. The major crystalline phase of TiO_2 was determined to be anatase, and the samples after doping with nitrogen show trace amount of brookite phase, which is attributed to chloride introduced in using ammonium chloride as nitrogen source. No iron oxide or Fe_xTiO_y peak could be observed in the XRD spectra, which suggests that all the iron ions were incorporated into the structures of titania and replaced titanium ion or located at interstitial site. The crystallite sizes of samples calculated using the Debye–Scherrer equation are about 10–12 nm.

X-ray based spectroscopies are useful in determining the chemical composition of materials. These techniques include X-ray absorption spectroscopy (XAS) such as extended X-ray absorption fine structure (EXAFS) and X-ray absorption near edge structure (XANES), X-ray fluorescence spectroscopy (XRF), energy dispersive X-ray spectroscopy (EDX), and X-ray photoelectron spectroscopy (XPS) [26, 27]. They are mostly based on detecting and analyzing radiation absorbed or emitted from a sample after excitation with X-rays, with the exception that electrons are analyzed in XPS. The spectroscopic features are characteristic of specific elements and thereby can be used for sample elemental analysis.

OPTICAL PROPERTIES AND SPECTROSCOPY OF NANOMATERIALS
© World Scientific Publishing Co. Pte. Ltd.
http://www.worldscibooks.com/nanosci/7093.html

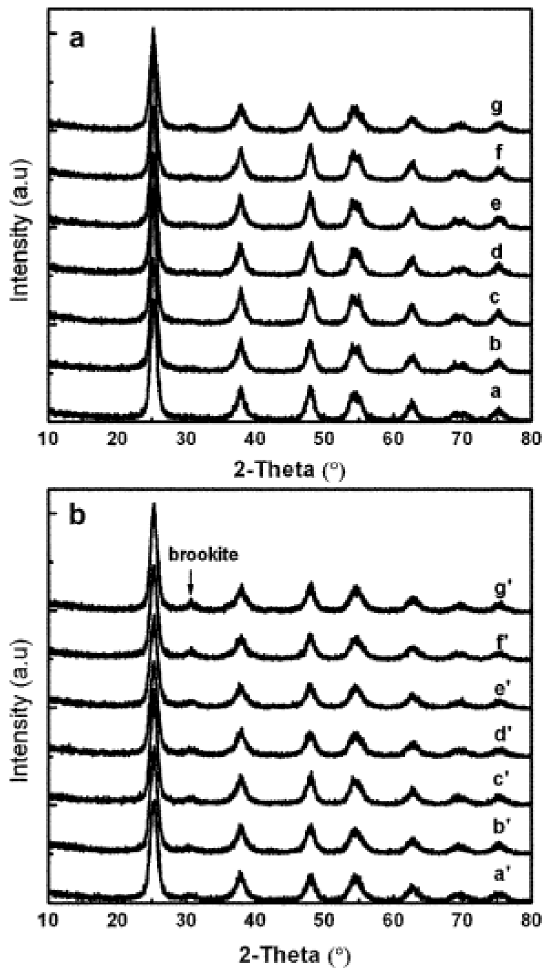

Fig. 3.9. X-ray diffraction patterns of xFe-TiO_2 (a) and N-*x*Fe-TiO_2 (b) with different Fe^{3+}-doping concentration: (a, a′) 0; (b, b′) 0.05%; (c, c′) 0.1%; (d, d′) 0.5%; (e, e′) 1.0%; (f, f′) 1.5%; (g, g′) 2.0%. Reproduced with permission from Ref. 25.

XPS is based on the measurement of the kinetic energy of photoelectrons generated when the sample is illuminated with soft (1.5 kV) X-ray radiation in an ultrahigh vacuum (UHV) [28]. If one X-ray photon with energy hν is used to excite an atom in its initial state with energy E_i and to eject an electron with kinetic energy, *KE*, with the atom resulting

OPTICAL PROPERTIES AND SPECTROSCOPY OF NANOMATERIALS
© World Scientific Publishing Co. Pte. Ltd.
http://www.worldscibooks.com/nanosci/7093.html

in a final state with energy E_f, one would have the following equation based on total energy conservation:

$$h\nu + E_i = KE + E_f \tag{3.2}$$

The difference between the photon energy and the electron kinetic energy is called the *binding energy* of the orbital from which the electron is ejected, which, based on Eq. (3.1), is equal to $E_f - E_i$. Since the photon energy is known from the X-ray radiation source used and the electron kinetic energy can be measured, the binding energy can be determined, which gives the energy difference between the final and initial states of the atom involved in the transition. This binding energy is characteristic for different orbitals of specific elements and is roughly equal to the Hartree–Fock energy of the electron orbital. Therefore, peaks in the photoelectron spectrum can be identified with specific atoms and surface composition can be analyzed. Because the photoelectrons are strongly attenuated by passage through the sample material itself, the information obtained comes from the sample surface, with a sampling depth on the order of 5 nm. Chemical bonding in molecules will cause binding energy shifts, which can thus be used to extract information of a chemical nature (such as atomic oxidation state) from the sample surface.

Figure 3.10 shows the XPS spectrum of Au/SiO_2 core/shell nanoparticles in the region corresponding to the binding energy range of 110–70 eV, which includes the Si 2p, Au 4f, and Cu 3p peaks recorded at 90° and 30° electron takeoff angles, respectively [29]. From the measured binding energies, the chemical elements can be easily identified as corresponding to $Au^{(0)}$ and Si^{4+}. To gain more information about the possible geometry-dependent composition, comparative studies were conducted on gold nanoparticles vapor-deposited onto a silicon substrate containing ca. 4-nm oxide layer. It was found that the XPS intensity ratio of peaks from elements of the core and the shell is independent of the electron takeoff angle, and bulk data are not very reliable for elucidating the composition, size, geometry of nanoparticles from XPS measurements.

XFS is similar to XPS in terms of the excitation mechanism but differs in its detection mechanism. While XPS detects photoelectrons, XFS detects

OPTICAL PROPERTIES AND SPECTROSCOPY OF NANOMATERIALS
© World Scientific Publishing Co. Pte. Ltd.
http://www.worldscibooks.com/nanosci/7093.html

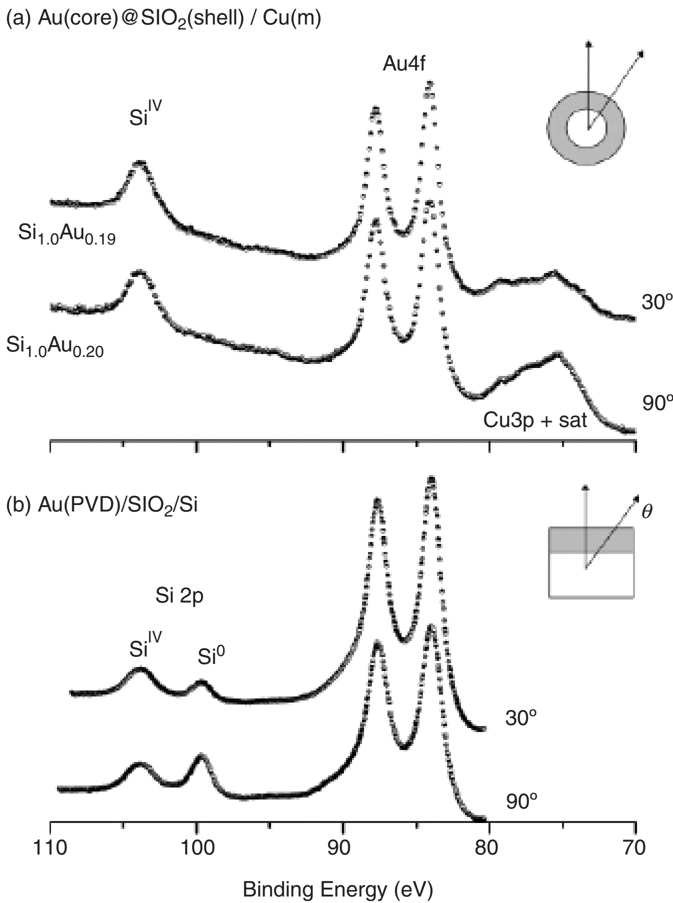

Fig. 3.10. The 110–70 eV region of the XPS spectrum recorded at 90° and 30° electron takeoff angles corresponding to (a) Au (core)/SiO_2 (shell) nanoparticles deposited on copper tape, (b) gold particles vapor-deposited (PVD) onto a silicon substrate containing ca. 4-nm oxide layer. Reproduced with permission from Ref. 29.

"secondary" or "fluorescent" X-rays from a material that has been excited by high-energy X-rays (or sometimes γ-rays) [30]. The principle behind XFS is relatively straightforward. When a material is exposed to high energy or short wavelength X-rays, ionization or electron ejection can take place if the X-ray photon energy is greater than its ionization energy. Due to the high energy of X-rays or γ-rays, tightly bound electrons in the

OPTICAL PROPERTIES AND SPECTROSCOPY OF NANOMATERIALS
© World Scientific Publishing Co. Pte. Ltd.
http://www.worldscibooks.com/nanosci/7093.html

inner, low energy orbitals of the atom in the material can be expelled. The resulting ionized atom is not unstable and electrons in outer, higher energy orbitals may fall or make a transition into the lower orbital to fill the hole left behind. In doing so, energy may be released in the form of a photon (usually with energy in the X-ray region still) with energy equal to the energy difference of the two orbitals involved. Because the orbitals are specific to individual atoms, the energy of the emitted photon that can be easily detected has energy characteristic of the atoms involved. The term "fluorescence" refers to the emitted X-ray photons, not visible light, even though visible light can also be generated and observed sometimes when a sample is subject to X-ray radiation.

Another powerful X-ray based spectroscopic technique is extended X-ray absorption fine structure (XAFS) [27]. EXFAS is based on measuring the fine structure near the absorption edge of a sample when subject to X-ray radiation. It is similar to UV-visible electronic absorption spectroscopy, in principle, except that the spectral range is in the X-ray region and EXAFS focuses on the fine structure specifically since it provides local structural information about specific atoms or ions. EXAFS relates to the details of how X-rays are absorbed by an atom at energies near and above the core-level binding energies of that atom. EXAFS measurements reflect the modulation of an atom's X-ray absorption probability due to the chemical and physical states of the atom. EXAFS spectra are especially sensitive to the formal oxidation state, coordination chemistry, and the local atomic structure of the selected element. One advantage of EXAFS is that it works for crystalline as well as noncrystalline or even highly disordered materials, including solutions. It is thus well suited for studying nanomaterials [31–34]. EXAFS measurements are relatively straightforward but require an intense and energy-tunable source of X-rays, which usually means the use of synchrotrons. While the experimental measurements can be simple, analysis of EXAFS data is somewhat involved and requires specific expertise and good knowledge of relevant physical principles. For convenience of data interpretation, the X-ray absorption spectrum is typically divided into two regimes: X-ray absorption near-edge spectroscopy (XANES) and extended X-ray absorption fine-structure spectroscopy (EXAFS). While XANES is more sensitive to formal oxidation state and coordination chemistry of the absorbing atom,

OPTICAL PROPERTIES AND SPECTROSCOPY OF NANOMATERIALS
© World Scientific Publishing Co. Pte. Ltd.
http://www.worldscibooks.com/nanosci/7093.html

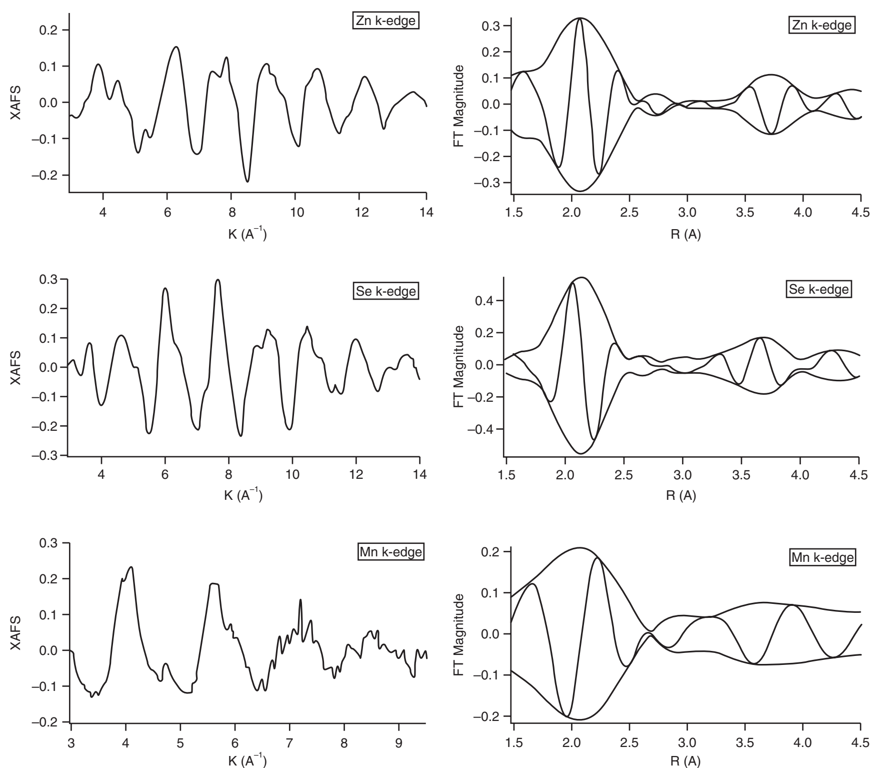

Fig. 3.11. XAFS (left) and FT-XAFS (right) traces for Mn^{2+}-doped ZnSe nanoparticles. The Fourier transform range is 3–14 Å^{-1} for the Zn K-edge and Se K-edge data and 3–9.5 Å^{-1} for the Mn K-edge. The XAFS data were collected at 20 K. Reproduced with permission from Ref. 35.

EXAFS is usually used to determine the distances, coordination number, and species of the neighbors of the absorbing atom.

Figure 3.11 shows some XAFS data for ZnSe:Mn nanoparticles [35]. By determining the local structure of the different ions in the nanoparticles, in conjunction with ESR data, and correlating to their optical properties, it was found that the Mn^{2+} ion is substitutional with tetrahedral symmetry inside the host ZnS nanoparticles and is luminescent around 580 nm, as expected, while Mn^{2+} ions on the nanoparticle surface have a different symmetry (octahedral) and are nonluminescent. This example

OPTICAL PROPERTIES AND SPECTROSCOPY OF NANOMATERIALS
© World Scientific Publishing Co. Pte. Ltd.
http://www.worldscibooks.com/nanosci/7093.html

shows the importance of simultaneous optical and structural studies in investigating nanomaterials.

A final example of X-ray related techniques useful for nanomaterials research is Small Angle X-ray Scattering (SAXS) [36, 37]. SAXS is an analytical technique often used for the structural characterization of solid and fluid materials in the nanometer range. In SAXS measurements, the sample is irradiated by a well-defined, monochromatic X-ray beam. Intensity distribution of the scattered beam at very small scattering angles is measured and it contains structural information of the scattering particles. SAXS can be used to study both monodisperse and polydisperse systems. Information about size, shape and internal structure of the particles can be determined for monodisperse systems and size distributions can be calculated for polydisperse systems. SAXS has been applied to investigate structural details of a variety of nanoparticles of inorganic, organic, as well as biological materials in the size range of 0.5 to 50 nm, usually with high intensity X-ray radiation.

3.3. Electrochemistry and photoelectrochemistry

Electrochemistry is another useful tool for characterizing electronic and electrochemical properties of nanomaterials [4, 38]. One major application is to determine the redox potentials or bandgaps with reference to a known potential or energy level, e.g. a known electrode such as Ag/AgCl or the standard hydrogen potential. This is more advantageous than optical measurement that usually only provide relative energy levels such as bandgap, but not on an absolute scale. Another key use is to determine charge transfer and transport properties in nanomaterials. Electrochemistry techniques have been used to study metal, semiconductor, and insulator or metal oxide nanostructures [39–45].

As example, electrochemistry techniques have been used to study the charging behavior of monodisperse gold nanoparticles, with 8 to 38 kilodaltons core mass or 1.1 to 1.9 nanometers in diameter, stabilized with short-chain alkanethiolate monolayers [46]. Figure 3.12 shows schematic STM double tunnel-junction model (a), electrochemical ensemble Coulomb staircase model (b), and differential pulse voltammograms for (c) butanethiolate (C4) and (d) hexanethiolate (C6) Au monolayer-protected metal clusters (MPCs) as a function of core size. The experimental results

OPTICAL PROPERTIES AND SPECTROSCOPY OF NANOMATERIALS
© World Scientific Publishing Co. Pte. Ltd.
http://www.worldscibooks.com/nanosci/7093.html

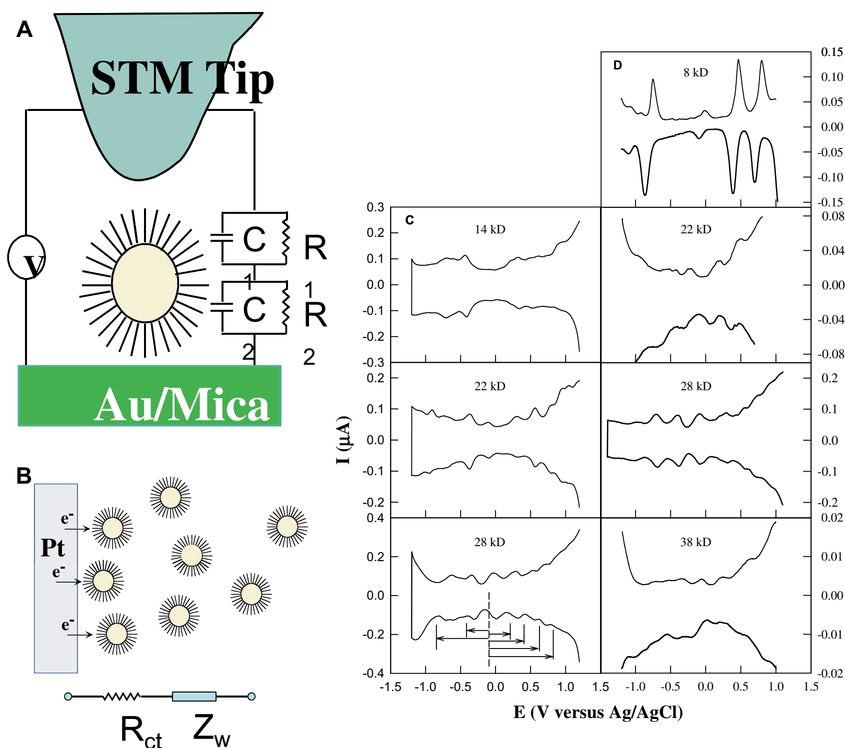

Fig. 3.12. Schematic STM double tunnel-junction model (a) and schematic electrochemical ensemble Coulomb staircase model (b). R_{ct} is charge transfer resistance and Z_W is diffusional (Warburg) impedance for MPC transport through the solution. Differential pulse voltammograms for (c) butanethiolate (C4) and (d) hexanethiolate (C6) Au MPCs as a function of uniform core size, in 0.05 M Hex_4NClO_4/toluene/acetonitrile (2/1 v:v), at 9.5×10^{-3} cm^2 Pt electrode; DC potential scan 10 mV/s, pulse amplitude 50 mV. Concentrations are: (c) 14 kD, 0.086 mM; 22 kD, 0.032 mM; 28 kD, 0.10 mM; (d) 8 kD, 0.30 mM; 22 kD, 0.10 mM; 28 kD, 0.10 mM; 38 kD, 0.10 mM. Reproduced with permission from Ref. 46.

show a transition from metal-like double-layer capacitive charging to redox-like charging as the core size decreases. This example demonstrates the usefulness of electrochemistry methods in studying nanomaterials.

Related to electrochemistry and spectroscopy is a more specialized technique called photoelectrochemistry (PEC). It is based on electrochemical measurements when one electrode, usually the anode, is subject to light illumination [47–52]. PEC is useful for studying nanomaterials that are

OPTICAL PROPERTIES AND SPECTROSCOPY OF NANOMATERIALS
© World Scientific Publishing Co. Pte. Ltd.
http://www.worldscibooks.com/nanosci/7093.html

active in photoelectochemical reactions. One example is hydrogen generation from water splitting that is attractive for solar energy conversion. The PEC technique involves measuring photocurrent in an electrochemical setup with light illumination on one or both electrondes (anode and cathode). A reference electrode is also used in a typical PEC setup. A more detailed discussion of PEC will be given in Chapter 10.

3.4. Nuclear magnetic resonance (NMR) and electron spin resonance (ESR)

3.4.1. *Nuclear magnetic resonance (NMR)*

Techniques based on magnetic resonance, such as NMR (nuclear magnetic resonance) and ESR (electron spin resonance), are also useful tools for materials characterization. NMR is particularly powerful for structural determination and is usually used to characterize molecules on the surface of nanomaterials as well as molecule–nanoparticle interaction.

The principle behind NMR is nuclear spin transitions in an applied external magnetic field [53]. Many nuclei have spin and all nuclei are electrically charged. If an external magnetic field is applied, energy transfer or transition is possible between the different nuclear spin energy levels. The transition takes place at a wavelength corresponding to radio frequencies (typically in the 40–800 MHz range). The signal that matches the transition, at the resonance frequency, is measured and processed in order to yield an NMR spectrum for the nucleus concerned. The resonant frequency of the transition energy is dependent on the effective magnetic field at the nucleus. This field is affected by electron shielding which is, in turn, dependent on the chemical environment. As a result, information about the nucleus' chemical environment can be derived from its resonant frequency. The most common nucleus probe in NMR is the proton, ^{1}H. For convenience, a chemical shift, δ, is defined for proton NMR as:

$$\delta = (\nu - \nu_0)/\nu_0 \tag{3.3}$$

where ν is the detected resonance frequency for the proton of interest and ν_0 = 400.13000000 MHz is the customarily adopted proton reference frequency of tetramethylsilane (TMS). For example, the NMR frequency

OPTICAL PROPERTIES AND SPECTROSCOPY OF NANOMATERIALS
© World Scientific Publishing Co. Pte. Ltd.
http://www.worldscibooks.com/nanosci/7093.html

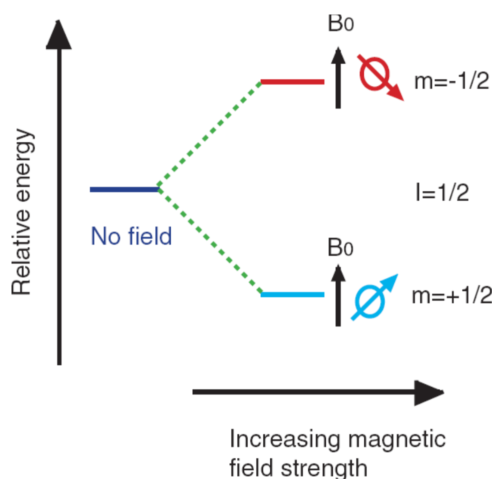

Fig. 3.13. Illustration of NMR transitions for a nuclear spin $I = 1/2$ system, e.g. a proton, under an applied external field.

of protons in benzene is 400.132869 MHz and its chemical shift is calculated to be 7.17 ppm based on Eq. (3.3). The chemical shift is usually expressed in ppm (part per million) for convenience.

The operating principle behind NMR is illustrated in Fig. 3.13, where transitions are shown between two nuclear spin states that split under an applied external magnetic field. The transition energy or the splitting between the two spins states is proportional to the applied magnetic field strength B_0. At higher frequency or field strength, the signal/noise ratio is better due to larger population difference between the ground and excited states.

NMR is a routine and powerful technique for structural determination and chemical analysis of organic and biological molecules including proteins and DNA. For nanomaterials research, NMR has often been used to identify or analyze molecules on the surface of nanomaterials or elements in the nanoparticle [54, 55]. For example, solid state ^{113}Cd, ^{77}Se, ^{13}C and ^{31}P NMR has been used to study a number of Cd chalcogenide nanoparticles synthesized in tri-n-octyl-phosphine (TOP) with different compositions and architectures. The pure CdSe and CdTe nanoparticles show a dramatic, size-sensitive broadening of the ^{113}Cd NMR line, which can be explained

OPTICAL PROPERTIES AND SPECTROSCOPY OF NANOMATERIALS
© World Scientific Publishing Co. Pte. Ltd.
http://www.worldscibooks.com/nanosci/7093.html

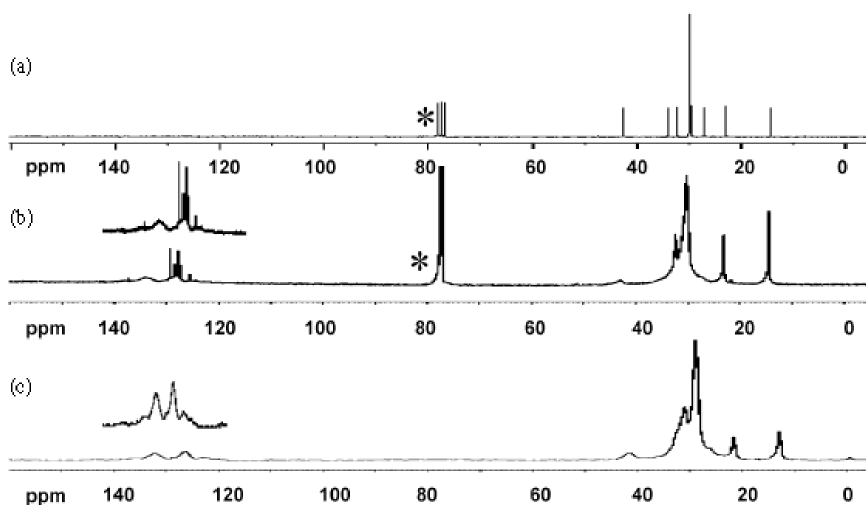

Fig. 3.14. (a) Solution ^{13}C spectra of HDA in $CDCl_3$*. (b) Solution ^{13}C spectra of 2-nm CdSe-HDA in $CDCl_3$*. This spectrum shows HDA on the surface of the particle as well as bound and unbound thiophenol. (c) Solid-state ^{13}C MAS of 2-nm CdSe-HDA shows the presence of HDA and thiophenol. The R-carbon of HDA is more pronounced than in solution and is at the same chemical shift as free HDA. Spinning speed is 12 kHz. Reproduced with permission from Ref. 55.

in terms of a chemical shift distribution arising from multiple Cd environments [56]. As another example, Fig. 3.14 shows ^{13}C NMR data on hexadecylamine (HDA)-passivated 2-nm CdSe in solution and the solid state [55]. A detailed analysis of these data, in conjunction with ^{1}H-^{113}Cd and ^{1}H-^{77}Se cross-polarization magic angle spinning (MAS) experiments performed on the Cd and Se atoms, provides a picture about the surface properties of the HDA-capped CdSe nanoparticles. It has been found that both HDA and thiophenol bind selectively to specific sites of the CdSe nanocrystal surface.

3.4.2. *Electron spin resonance (ESR)*

Another, somewhat more specialized, technique based on magnetic resonance is ESR (electron spin resonance), also called EPR (electron paramagnetic resonance) [57]. ESR is similar to NMR except that the spin

OPTICAL PROPERTIES AND SPECTROSCOPY OF NANOMATERIALS
© World Scientific Publishing Co. Pte. Ltd.
http://www.worldscibooks.com/nanosci/7093.html

is based on the electron rather than nuclei and the frequency range for electron spin transitions is in the range of microwave frequency (GHz), as compared to NMR in the lower radio frequency (MHz). ESR is based on measuring transitions in molecules, ions or atoms possessing electrons with unpaired spins, i.e. electronic spin $S > 0$, under an external magnetic field. With ESR, energy is absorbed by the sample when the frequency of the radiation is on resonance with the energy difference between two spin states of the electrons in the sample and the appropriate selection rules are satisfied.

Most materials in a bulk form at normal conditions have net zero electronic spin and are thus ESR silent. ESR activity is observed in a number of situations where unpaired electrons are involved or the net electronic spin is not zero, e.g. transition-metal and rare-earth species that contain unpaired n*d* and/or m*f* electrons, organic free radicals, such as 1, 1′-Diphenyl-2-picryl-hydrazyl (DPPH) and 2, 2, 6, 6-tetramethyl-1-piperidinyloxyl (TEMPO), organic ion-radicals created during redox reactions, and triplet state organic molecules and biradicals.

The principle of transition in ESR is illustrated in Fig. 3.15 Two electron spin states are split into two nondegenerate states under an applied

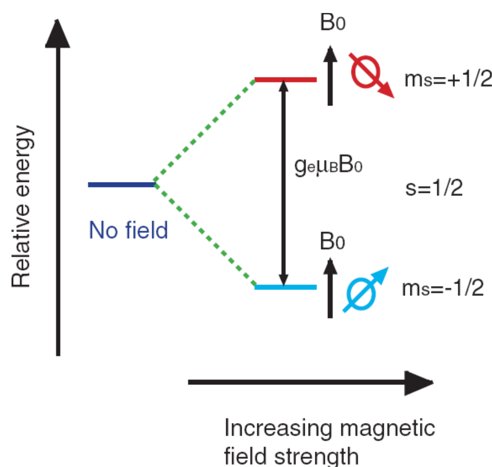

Fig. 3.15. Illustration of electron spin transitions under an external magnetic field B_0, where g_e is the so-called g-factor, a constant around 2 for the free electron, and μ_B is the Bohr magneton, which is equal to $eh/4\pi m_e = 9.2740 \times 10^{-24}$ J/T.

OPTICAL PROPERTIES AND SPECTROSCOPY OF NANOMATERIALS
© World Scientific Publishing Co. Pte. Ltd.
http://www.worldscibooks.com/nanosci/7093.html

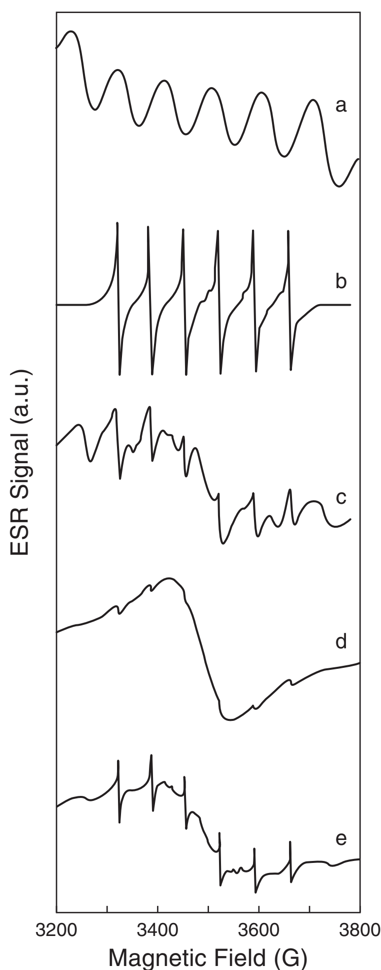

Fig. 3.16. ESR spectra of Mn^{2+}/USY (a), ZnS:Mn^{2+}/USY (b) and different sized ZnS:Mn nanoparticles: (c) 3.5 nm, (d) 4.5 nm and (e) 10 nm. USY is for ultrastable zeolite Y. Reproduced with permission from Ref. 59.

external magnetic field. Under resonance conditions, transitions can occur between these two states, resulting in absorption of electromagnetic radiation, usually in the microwave frequency range. Similar to NMR, the transition energy or the splitting between the two spins states is proportional to the applied magnetic field strength B_0. At higher frequency or

OPTICAL PROPERTIES AND SPECTROSCOPY OF NANOMATERIALS
© World Scientific Publishing Co. Pte. Ltd.
http://www.worldscibooks.com/nanosci/7093.html

field strength, the signal/noise ratio is better due to larger population difference between the ground and excited states. For similar reason, ESR is more sensitive than NMR due to the higher frequency or larger excited and ground state population difference in ESR than NMR.

In nanomaterials research, ESR is particularly useful for studying species with unpaired electrons such as dopants in nanomaterials [35, 58–61]. For example, Fig. 3.16 shows the ESR spectra of Mn^{2+} in different environment, ultrastable zeolite Y (USY) and ZnS nanoparticles in USY, and different sized ZnS nanoparticles [59]. It is clear that the ESR patterns observed for Mn^{2+} are very sensitive to their host environment.

Another interesting application of ESR is to study species with unpaired electrons on nanomaterials surface, such as radicals. For example, radicals on CdSe QD surfaces have been studied by ESR along with optical spectroscopy to understand electron transfer from QD to the radical [62, 63], as will be discussed in more detail in Chapter 4.

3.5. Summary

This chapter provides a brief survey of experimental techniques that are not based on optical spectroscopy but useful for characterizing different properties of nanomaterials, including X-ray (XRD, XAFS, XFS, XPS), microscopy (STM, AFM, TEM, and SEM), electrochemistry, NMR and ESR. They are important for determining topology, morphology, surface, chemical composition and crystal structures of nanomaterials. These techniques complement optical spectroscopy that provides optical, electronic as well as structural information. Given the complex nature of nanomaterials, it is common that a combination of these experimental techniques is used to gain a complete picture and understanding of their properties.

One example is the distinction between so-called "core/shell" structures versus aggregates in the case of gold nanostructures from the reaction of $HAuCl_4$ and Na_2S [64]. While the initial and several follow-up reports claimed Au_2S/Au core/shell structure mainly based on spectroscopic evidence [65, 66], more detailed subsequent studies using a combination of optical and structural characterization techniques, including EXAFS, SAXS and TEM, have shown that the reaction product is

OPTICAL PROPERTIES AND SPECTROSCOPY OF NANOMATERIALS
© World Scientific Publishing Co. Pte. Ltd.
http://www.worldscibooks.com/nanosci/7093.html

mostly aggregates of gold nanoparticles [67–69]. This example shows that high quality, direct structural studies are essential for unambiguously determining the structure of nanomaterials.

References

1. G.Y. Liu, S. Xu and Y.L. Qian, *Acc. Chem. Res*. **33**, 457 (2000).
2. Z.L. Wang, *J. Phys. Chem. B* **104**, 1153 (2000).
3. Z.L. Wang, P. Poncharal and W.A. de Heer, *Microscopy and Microanalysis* **6**, 224 (2000).
4. J.Z. Zhang, Z.L. Wang, J. Liu, S. Chen and G.-y. Liu, *Self-assembled Nanostructures*. Nanoscale Science and Technology, New York: Kluwer Academic/Plenum Publishers. **316** (2003).
5. G. Cao, *Nanostructures & Nanomaterials: Synthesis, Properties & Applications*, London: Imperial College Press. **433** (2004).
6. F.J. Giessibl, S. Hembacher, H. Bielefeldt and J. Mannhart, *Science* **289**, 422 (2000).
7. D. Bonnell, *Scanning Probe Microscopy and Spectroscopy: Theory, Techniques, and Applications*, New York: Wiley-VCH (2000).
8. E. Meyer, *Atomic Force Microscopy: Fundamentals to Most Advanced Applications* Vol. 1, New York: Springer-Verlag TELOS. **250** (2007).
9. G. Binnig, C.F. Quate and C. Gerber, *Phys. Rev. Lett.* **56**, 930 (1986).
10. H.J. Guntherodt, D. Anselmetti and E. Meyer, eds. NATO ASI series. Series E, Applied sciences. Vol. 286, Kluwer Academic. **644** (1995).
11. F.J. Giessibl, H. Bielefeldt, S. Hembacher and J. Mannhart, *Annalen Der Physik* **10**, 887 (2001).
12. C. Bai, *Scanning Tunneling Microscopy and Its Applications*, New York: Springer-Verlag TELOS. **366** (2007).
13. A.M. Baro, G. Binnig, H. Rohrer, C. Gerber, E. Stoll, A. Baratoff and F. Salvan, *Phys. Rev. Lett.* **52** 1304 (1984).
14. A. Riposan and G.Y. Liu, *J. Phys. Chem. B* **110**, 23926 (2006).
15. J.I. Goldstein, D.E. Newbury, P. Echlin, D.C. Joy, J. Romig, A.D., C.E. Lyman, C. Fiori and E. Lifshin, *Scanning Electron Microscopy and X-ray Microanalysis*. 2nd ed, New York: Plenum Press. **820** (1992).
16. N. Hanada, E. Hirotoshi, T. Chikawa, E. Akiba and H. Fujii, *J. Alloy Compd.* **450**, 395 (2008).
17. Z.L. Liu, J.C. Deng, J.J. Deng and F.F. Li, *Materials Science and Engineering B-Advanced Functional Solid-State Materials* **150**, 99 (2008).

OPTICAL PROPERTIES AND SPECTROSCOPY OF NANOMATERIALS
© World Scientific Publishing Co. Pte. Ltd.
http://www.worldscibooks.com/nanosci/7093.html

18. Z.L. Wang, ed., Wiley-VCH: New York. **406** (2000).
19. Z.L. Wang, *Advan. Mater.* **10**, 13 (1998).
20. N.S. Yu, X.P. Hao, X.G. Xu and M.H. Jiang, *Mater Lett*. **61**, 523 (2007).
21. R.L. Whetten, J.T. Khoury, M.M. Alvarez, S. Murthy, I. Vezmar, Z.L. Wang, P.W. Stephens, C.L. Cleveland, W.D. Luedtke and U. Landman, *Advan. Mater.* **8**, 428 (1996).
22. C.B. Murray, C.R. Kagan and M.G. Bawendi, *Science* **270**, 1335 (1995).
23. C.B. Murray, C.R. Kagan and M.G. Bawendi, *Ann. Rev. Mater. Sci.* **30**, 545 (2000).
24. A.P. Alivisatos, *Science* **271**, 933 (1996).
25. Y. Cong, J.L. Zhang, F. Chen, M. Anpo and D.N. He, *J. Phys. Chem. C* **111**, 10618 (2007).
26. T.L. Barr, *Modern ESCA: The Principles and Practice of X-Ray Photoelectron Spectroscopy*, New York: CRC Press. **384** (1994).
27. D.C. Koningsberger and R. Prins, eds. A Series of Monographs on Analytical Chemistry and Its Applications, Wiley-Interscience: New York. **688** (1988).
28. T.L. Barr, *Modern ESCA: The Principles and Practice of X-Ray Photoelectron Spectroscopy*, Boca Raton, FL: CRC Press. **376** (2008).
29. I. Tunc, S. Suzer, M.A. Correa-Duarte and L.M. Liz-Marzan, *J. Phys. Chem. B* **109**, 7597 (2005).
30. J.A. Carlisle, S.R. Blankenship, R.N. Smith, A. Chaiken, R.P. Michel, T. van Buuren, L.J. Terminello, J.J. Jia, T.A. Callcott and D.L. Ederer, *J. Clust. Sci.* **10**, 591 (1999).
31. H. Hosokawa, H. Fujiwara, K. Murakoshi, Y. Wada, S. Yanagida and M. Satoh, *J. Phys. Chem*. **100**, 6649 (1996).
32. J. Rockenberger, L. Troger, A. Kornowski, T. Vossmeyer, A. Eychmuller, J. Feldhaus and H. Weller, *J. Phys. Chem. B* **101**, 2691 (1997).
33. R.E. Benfield, D. Grandjean, M. Kroll, R. Pugin, T. Sawitowski and G. Schmid, *J. Phys. Chem. B* **105**, 1961 (2001).
34. Y.V. Zubavichus, Y.L. Slovokhotov, M.K. Nazeeruddin, S.M. Zakeeruddin, M. Gratzel and V. Shklover, *Chem. Mater.* **14**, 3556 (2002).
35. T.J. Norman, D. Magana, T. Wilson, C. Burns, J.Z. Zhang, D. Cao and F. Bridges, *J. Phys. Chem. B* **107**, 6309 (2003).
36. O. Glatter and O. Kratky, eds., Acamemic Press: New York. **515** (1982).
37. S. Remita, P. Fontaine, E. Lacaze, Y. Borensztein, H. Sellame, R. Farha, C. Rochas and M. Goldmann, *Nuclear Instruments & Methods in Physics Research Section B-Beam Interactions with Materials and Atoms* **263**, 436 (2007).

OPTICAL PROPERTIES AND SPECTROSCOPY OF NANOMATERIALS
© World Scientific Publishing Co. Pte. Ltd.
http://www.worldscibooks.com/nanosci/7093.html

38. G. Hodes, Wiley-VCH: Weinheim; New York. **326** (2001).
39. C. Lebreton and Z.Z. Wang, *Surface Sci.* **382**, 193 (1997).
40. C. Schonenberger, B.M.I. vanderZande, L.G.J. Fokkink, M. Henny, C. Schmid, M. Kruger, A. Bachtold, R. Huber, H. Birk and U. Staufer, *J. Phys. Chem. B* **101**, 5497 (1997).
41. W. Chen and S.G. Sun, *Spectroscopy and Spectral Analysis* **24**, 817 (2004).
42. J. Meier, J. Schiotz, P. Liu, J.K. Norskov and U. Stimming, *Chem. Phys. Lett.* **390**, 440 (2004).
43. X.H. Guan, Y.H. Qin, S.Y. Zhang, J. Guo and J.H. Li, *Chemical J. Chinese Universities-Chinese* **26**, 1825 (2005).
44. L. Zhang, Q. Zhang, X.B. Lu and J.H. Li, *Biosens. Bioelectron.* **23**, 102 (2007).
45. W. Sun, R.F. Gao and K. Jiao, *J. Phys. Chem. B* **111**, 4560 (2007).
46. S.W. Chen, R.S. Ingram, M.J. Hostetler, J.J. Pietron, R.W. Murray, T.G. Schaaff, J.T. Khoury, M.M. Alvarez and R.L. Whetten, *Science* **280**, 2098 (1998).
47. C. Nasr, S. Hotchandani, W.Y. Kim, R.H. Schmehl and P.V. Kamat, *J. Phys. Chem. B* **101**, 7480 (1997).
48. Y.Q. Wang, H.M. Cheng, Y.Z. Hao, J.M. Ma, B. Xu, W.H. Li and S.M. Cai, *J. Mater. Sci. Lett.* **18**, 127 (1999).
49. P.V. Kamat, S. Barazzouk, S. Hotchandani and K.G. Thomas, *Chem. Eur. J.* **6**, 3914 (2000).
50. L. Zhang, Y.Q. Wang, M.Z. Yang, E.Q. Gao and S.M. Cai, *Chemical J. Chinese Universities-Chinese* **21**, 1075 (2000).
51. I. Willner, F. Patolsky and J. Wasserman, *Angew. Chem. Int. Edit* **40**, 1861 (2001).
52. T. Lana-Villarreal and R. Gomez, *Electrochem. Commun.* **7**, 1218 (2005).
53. J.B. Lambert and E.P. Mazzola, *Nuclear Magnetic Resonance Spectroscopy: an Introduction to Principles, Applications, and Experimental Methods*, Upper saddle River, NJ: Pearson/Prentice Hall. **341** (2004).
54. O. Kohlmann, W.E. Steinmetz, X.A. Mao, W.P. Wuelfing, A.C. Templeton, R.W. Murray and C.S. Johnson, *J. Phys. Chem. B* **105**, 8801 (2001).
55. M.G. Berrettini, G. Braun, J.G. Hu and G.F. Strouse, *J. Am. Chem. Soc*. **126**, 7063 (2004).
56. C.I. Ratcliffe, K. Yu, J.A. Ripmeester, M.B. Zaman, C. Badarau and S. Singh, *Phys. Chem. Chem. Phys.* **8**, 3510 (2006).
57. M.R. Brustolon, *Principles and Applications of Electron Paramagnetic Resonance Spectroscopy*, New York: Blackwell Publishers. **400** (2008).
58. P.H. Borse, D. Srinivas, R.F. Shinde, S.K. Date, W. Vogel and S.K. Kulkarni, *Phys. Rev. B* (Condensed Matter), **60**, 8659 (1999).

OPTICAL PROPERTIES AND SPECTROSCOPY OF NANOMATERIALS
© World Scientific Publishing Co. Pte. Ltd.
http://www.worldscibooks.com/nanosci/7093.html

59. W. Chen, R. Sammynaiken, Y.N. Huang, J.O. Malm, R. Wallenberg, J.O. Bovin, V. Zwiller and N.A. Kotov, *J. Appl. Phys.* **89**, 1120 (2001).
60. V.N. Andreev, S.E. Nikitin, V.A. Klimov, S.V. Kozyrev, D.V. Leshchev and K.F. Shtel'makh, *Phys. Solid State* **43**, 788 (2001).
61. P. Balaz, M. Valko, E. Boldizarova and J. Briancin, *Mater. Lett.* **57**, 188 (2002).
62. V. Maurel, M. Laferriere, P. Billone, R. Godin and J.C. Scaiano, *J. Phys. Chem. B* **110**, 16353 (2006).
63. E. Heafey, M. Laferriere and J.C. Scaiano, *Photochem. Photobiol. Sci.* **6**, 580 (2007).
64. J.Z. Zhang, A.M. Schwartzberg, T. Norman, C.D. Grant, J. Liu, F. Bridges and T. van Buuren, *Nano Lett.* **5**, 809 (2005).
65. H.S. Zhou, I. Honma, H. Komiyama and J.W. Haus, *Phys. Rev. B-Condensed Matter* **50**, 12052 (1994).
66. R.D. Averitt, D. Sarkar and N.J. Halas, *Phys. Rev. Lett.* **78**, 4217 (1997).
67. T.J. Norman, C.D. Grant, A.M. Schwartzberg and J.Z. Zhang, *Opt. Mater.* **27**, 1197 (2005).
68. A.M. Schwartzberg, A. Wolcott, T. Willey, T. Van Buuren and J.Z. Zhang, *SPIE Proc*. **5513**, 213 (2004).
69. A.M. Schwartzberg, C.D. Grant, T. van Buuren and J.Z. Zhang, *J. Phys. Chem. C* **111**, 8892 (2007).

OPTICAL PROPERTIES AND SPECTROSCOPY OF NANOMATERIALS
© World Scientific Publishing Co. Pte. Ltd.
http://www.worldscibooks.com/nanosci/7093.html